A novel CFD approach for the computation of R744 flashing nozzles in compressible and metastable conditions

A novel CFD approach for the computation of R744 flashing nozzles in compressible and metastable conditions

Francesco Giacomelli*, Federico Mazzelli*, Adriano Milazzo*

*Department of Industrial Engineering (DIEF), University of Florence, 50139 Florence, Italy

francesco.giacomelli@unifi.it

ABSTRACT

The present paper describes a novel CFD approach for the flashing of CO_2 through nozzles and ejectors. The novelty of the method is represented by the possibility of defining both the liquid and vapor phases as compressible materials. The properties of each phase are obtained via look-up tables calibrated against standard fluid libraries and are valid in the whole domain of interest, including the supercritical, subcritical and metastable regions.

The model has been implemented within a commercial CFD solver and is completely general, i.e., it can be applied to any type of compressible multiphase flow. In the present study, the proposed approach has been validated against an experimental test-case available in literature.

Keywords: R744, flashing Nozzle, CFD, look-up tables, metastable properties

Nomenclature		Greek letters	
a	Speed of sound (m s^{-1})	α	Volume fraction
E	Energy	β	Mass fraction of the phase
f, g	Functions in Eq. 9	Γ	Source term
h	Enthalpy (kJ kg^{-1})	ε	Rate of turbulence dissipation
k	Turbulence kinetic energy	θ	Angle of diverging nozzle (°)
p	Pressure (Pa)	ρ	Density (kg m^{-3})
q	Conductive heat transfer	ς	Mass-specific thermodynamic property
T	Temperature (K)	τ	Shear stress (Pa)
t	Time (s)	χ	Volume-specific thermodynamic property
x	Coordinate (m)		
Y	Mass fraction of the species		
Superscripts/subscripts		Acronyms	
c	Condensation	CFD	Computational Fluid Dynamics
e	Evaporation	EOS	Equation Of State
eff	Effective	EXP	Experimental
l	Liquid	HEM	Homogeneous Equilibrium Model
m	Mixture	HFO	Hydro-Fluoro-Olefin
sat	Saturation	SST	Shear Stress Transport
v	Vapor	UDF	User Defined Function
		UDRGM	User Defined Real Gas Model

1. INTRODUCTION

The use of ejectors to improve the efficiency and capacity of vapor compression chillers has seen a renewed interest from both industry and academy in recent years. One of the fluids that benefits the most from the modification of the conventional cycle (e.g., by the inclusion of a two-phase flashing ejector) is carbon dioxide. The use of ejectors in R744 vapor compression cycles was first proposed by Lorentzen [1] and widely tested both numerically and experimentally (e.g. [2] and [3] to cite some). These early studies demonstrated significant efficiency and capacity improvements despite the low additional investment cost.
One of the most common cycle improvement is shown in Figure 1, where the ejector is used to compress the low-pressure vapor from the evaporator to the receiver, thus reducing the pressure ratio of the compressor. A further benefit of the ejector is the increase in system capacity thanks to the reduction of the throttling losses faced by the flow coming from the gas cooler (or condenser).

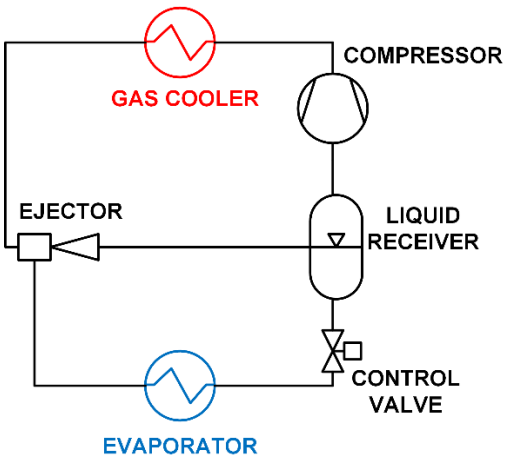

Figure 1: vapor compression cycle equipped with ejector

The main challenge in the research and development of the ejector is the understanding and modeling of the complex flow occurring in such a device. Some of the typical features are, for instance, two-phase non-equilibrium flow with phase change, presence of shocks and expansion-waves, recirculation, supersonic mixing layer between motive and suction flows. Consequently, the development and validation of predictive CFD models is necessary in order to enhance the performance of these devices.
To date, several CFD studies on two-phase flashing ejector have already been conducted, but more work has still to be done in order to improve the currently available models. In the work of Yazdani et al. [4] the authors used a "Mixture-Model" approach to simulate the flow of CO_2 within flashing ejectors. Basically, this is a single phase model with the solution of the volume fraction transport equation of the vapor phase. The model is capable to account for the non-equilibrium phase change in the ejector and the authors implemented it in the commercial code ANSYS Fluent. Lucas et al. [5] used a homogeneous equilibrium model (HEM) with the phase change occurring in equilibrium and the two phases sharing same pressure and temperature; in this case, the model was implemented within the open source CFD code Open-FOAM. In Smolka et al. [6] the authors employed a HEM based on a modified enthalpy transport equation implemented in the commercial code ANSYS Fluent. A similar approach was used by Giacomelli et al. in [7] and [8] who evaluated the fluid properties through a bi-linear interpolation of lookup-tables. The tables were automatically generated by means of a Matlab [9] script linked with the NIST Refprop v.9.0 libraries.
In 2011, Colarossi [10] developed a Homogeneous Relaxation Model (HRM) and implemented it within the CFD code Open-FOAM. A similar model was also developed in ANSYS Fluent by Haida et al. [11], by modifying the previously validated HEM.
The present work presents a new approach that treats both the liquid and vapor phases as compressible materials. The method was developed within the CFD package ANSYS Fluent v19.0 [12] and is based on the construction of dedicated R744 look-up tables and their extension in the metastable region. The computational results are compared against the experimental data obtained by Nakagawa et al. [13] for a R744 flashing nozzle.

2. NUMERICAL MODEL

The numerical model is based on a single fluid approach, also known as Mixture-Model. The set of averaged conservation equations for mass, momentum and energy has the following form:

$$\begin{aligned}
&\frac{\partial \rho_m}{\partial t} + \frac{\partial \rho_m u_{mj}}{\partial x_j} = 0 \\
&\frac{\partial \rho_m u_{mi}}{\partial t} + \frac{\partial \rho_m u_{mi} u_{mj}}{\partial x_j} = -\frac{\partial p}{\partial x_j} + \frac{\partial \tau_{ij_eff}}{\partial x_j} \\
&\frac{\partial \rho_m E_m}{\partial t} + \frac{\partial \rho_m u_{mj} h_m}{\partial x_j} = \frac{\partial q_{j_eff}}{\partial x_j} + \frac{\partial u_{mi} \tau_{ij_eff}}{\partial x_j} \\
&\frac{\partial \rho_v \alpha_v}{\partial t} + \frac{\partial \rho_v u_{mj} \alpha_v}{\partial x_j} = \Gamma_e - \Gamma_c
\end{aligned} \qquad (1)$$

The subscript *m* refers to mixture properties that are calculated by means of mass or volume weighted averages as follows:

$$\begin{aligned}
&\varsigma_m = \beta_l \varsigma_l + (1 - \beta_l)\varsigma_v \\
&\chi_m = \alpha_l \chi_l + (1 - \alpha_l)\chi_v
\end{aligned} \qquad (2)$$

The subscripts *l* and *v* refer to liquid and vapor properties, β_l is the liquid phase mass fraction, α_l is the liquid volume fraction, ς_m represents mixture thermodynamic properties like enthalpy, entropy, total energy, etc. and χ_m denotes either the mixture density, molecular viscosity or thermal conductivity.
The problem involves a two-phase mixture, so the following relation is valid:

$$\alpha_v + \alpha_l = 1 \qquad (3)$$

Since the flow is expected to be supersonic or near the sonic conditions, the definition of the two-phase sound speed requires special consideration. The definition of this property of the flow is not accessible and modifiable by the user of ANSYS Fluent but, as already reported in [14], the following equation was found to be used by the solver:

$$a = \sqrt{\frac{1}{(\alpha_l \rho_l + \alpha_v \rho_v)\left(\frac{\alpha_l}{\rho_l a_l^2} + \frac{\alpha_v}{\rho_v a_v^2}\right)}} \qquad (4)$$

This equation represents the harmonic-average of the sound speeds of saturated phases [15] and is commonly used in many CFD applications, especially for water and steam mixtures ([14], [16] and [17]). Finally, the effect of slip velocity between the phases is neglected, and the phases are assumed to share the same pressure and temperature (mechanical and thermal equilibrium conditions). Hence, the following identities are valid in the whole domain:

$$\begin{aligned}
&u_v = u_l = u_m \\
&p_v = p_l = p \\
&T_v = T_l = T
\end{aligned} \qquad (5)$$

Γ_e and Γ_c in the last equation of (1) are the mass-transfer source terms related to the evaporation and condensation process respectively. The two terms can be written in the following form:

$$\Gamma_e = \sigma_e \alpha_l \rho_l \frac{T - T_{sat}}{T_{sat}} \quad (6)$$

Which is valid if T > T_{sat}; else if T < T_{sat} one has:

$$\Gamma_c = \sigma_c \alpha_v \rho_v \frac{T - T_{sat}}{T_{sat}} \quad (7)$$

σ_e and σ_c are two accommodation coefficients that can be interpreted as relaxation times [12] and can have different values for condensation and evaporation. From now on these coefficients will be referred to as evaporation and condensation factor, respectively. The saturation temperature in Equations 6 and 7 is calculated as a polynomial function of the static pressure natural logarithm and implemented into Fluent by means of a UDF.

The phase change model is obtained by substituting the Clausius-Clayperon equation into the Hertz-Knudsen equation. For more details on the derivation and the physical basis of the model the reader is referred to [12] and [18]. The described model is available in ANSYS Fluent as a standard mass-transfer model.

To date, more accurate methods exist that employ either Mixture or full Eulerian-Eulerian multiphase approaches. These methods have been extensively used to simulate the flashing of water, e.g. in [19], [20] and [21]. In this case, detailed experimental data are abundant in the literature, which allows a proper calibration of the several unknown parameters that characterize the mass, momentum and heat transfer between the liquid and vapor phases. More details on recent advancements in the numerical modeling of flashing water flow can be found in the review of Liao and Lucas [21] and in the work of Karathanassis et al. [22].

Unfortunately, experimental test cases for CO_2 flow are still lacking. In particular, new experiments are needed that can provide simultaneous evidence of wall temperature and pressure profiles, mass flow rates measurements, local bubble density and diameters, as well as insights on the wall conditions. Therefore, the model adopted in the present work is a standard Mixture Model that allows avoiding the calibration of a great number of unknown parameters. This new procedure is completely general and it can easily be adapted to any fluid in both single and two-phase flows.

2.1 EOS and transport Properties

The evaluation of the fluid thermodynamic properties in compressible multiphase flow is a topic of primary importance. The inaccurate evaluation of these properties can lead to significant deviation with respect to actual mass flow rate and local pressure or temperature trends. This issue is even more critical for CO_2 due to the extremely high pressure variations typical of nozzle and ejector flows. The solution to this problem generally requires the definition of two compressible materials, one for each phase.

The best way to define the properties for a compressible phase in ANSYS Fluent is to adopt a *User-Defined Real Gas Model* (UDRGM), which is a set of C programming language function that can be edited by the user. However, in multiphase flows only one UDRGM can be adopted, e.g., the liquid phase. The definition of the vapor properties is thus subjected to some limitations; most notably, the isobaric specific heat capacity and specific enthalpy must be function of temperature only. In principle, this is not a very stringent restriction when the liquid or vapor phase are far from the critical state. However, in HVAC applications the flow of CO_2 is often transcritical and the fluid properties undergo large variations with respect to both temperature and pressure. A workaround to this problem consists in the use of a Multispecies-UDRGM.

The adoption of this scheme within the Fluent multiphase solver allows defining a UDRGM for both the liquid and vapor phases. In order to accomplish this, two different *species* and two different *phases* must be defined, as described in Figure 2. The first of the two *species* has the properties of the liquid CO_2 and it is named the "liquid species". The second *species* has the properties of vapor and it is called the "vapor species". The properties of two species are coded inside a unique *Multispecies-UDRGM* file. This file is then duplicated to express the properties of both the liquid and vapor.

This procedure activates four species, two of which must be considered as "dummy". In order to do this, the *mass* fraction Y of each species (in the domain of the corresponding phase) at the nozzle boundaries is set to a constant value that is either 1 or 0. Moreover, the mass transfer mechanisms due to evaporation or condensation is activated only for the two species of interest. Finally, unphysical diffusion between the species is suppressed by setting the molecular diffusivity of each material to a nearly-zero value and by imposing a very large turbulent Schmidt number (this is needed for the turbulent model). As a result, the final set of equations correspond to the Mixture-Model equations described in the previous section.

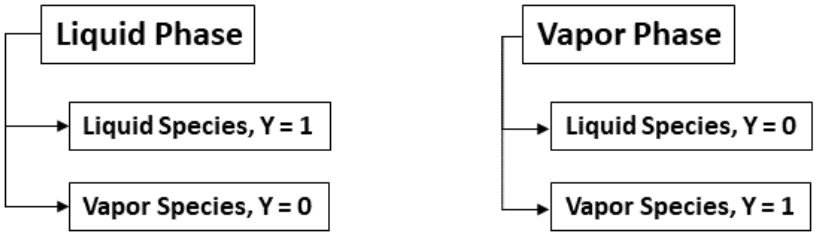

Figure 2: multispecies multiphase model layout

In order to obtain an accurate and computationally efficient approach the properties of both phases are inserted in the multispecies-UDRGM by means of 22 lookup-tables. As reported in [23] [24] [7] [25], this method is a practical and common solution for CFD simulations.
In the present model, all the lookup-tables have been automatically generated through a VBA Excel code and printed in ASCII text files. The code is directly linked with the NIST Refprop libraries [26], which use the Span and Wagner equation of state (EOS) for the properties of R744 [27]. This EOS makes use of the Helmholtz-free-energy potential and represents the current state of the art for the description of CO_2 properties. It is worth to mention that the properties calculated with this method can be extended in both the liquid and vapor metastable regions, up to the respective spinodal lines (for further details on how to calculate metastable properties with Nist Refprop, the reader is referred to [26]). .
As an example, Figure 3 shows the density map for the liquid phase, as obtained from the corresponding look-up table. The metastable states are included in the region that lies between the saturation line (in red) and the spinodal limit. Beyond this limit, the NIST database would return a non-value, which can produce abrupt interruption of the fluid properties definition. Therefore, an extrapolation of the properties beyond the spinodal line (not shown in Figure 3) was necessary in order to avoid numerical errors during the first iterations (this problem is discussed in section 4). The steps sizes in terms of Temperature and Pressure are respectively 1 K and 0.1 MPa and they are kept constants in the whole domain. A more computationally efficient approach would be to implement a variable step size as adopted in the work by De Lorenzo et al. [23]. However, sensitivity analyses performed on the look-up table step size (see later) has revealed that an adequate level of accuracy can be achieved without an excessive refinement and computational cost. Therefore, this method was adopted in the present work.

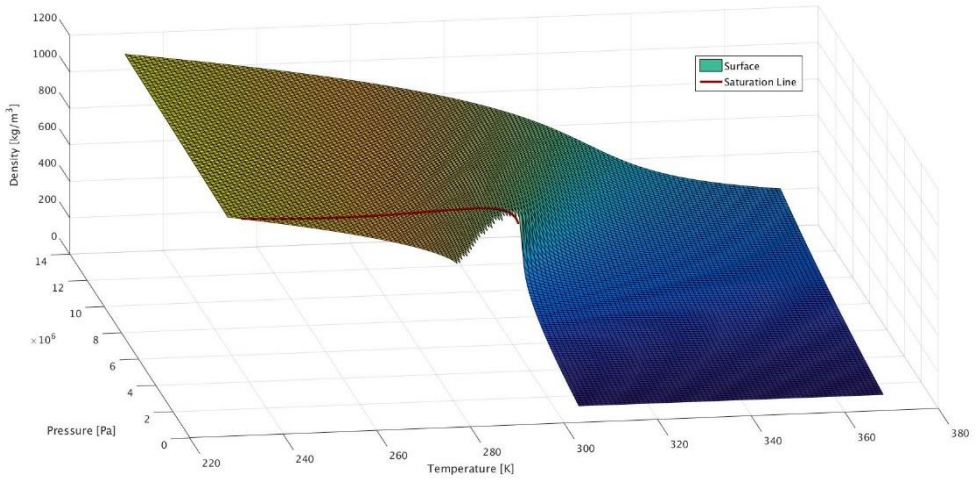

Figure 3: Density lookup-table as function of pressure and temperature with saturation line

All the lookup-tables are read and loaded in the Random Access Memory (RAM) before the start of the calculation. At runtime the solver operates bi-linear interpolations (similarly to [28]) in terms of pressure and temperature to calculate the local value of the various properties. The procedure of loading and interpolating the tables is developed by means of C code programming with a total of 44 additional functions included in the header files of the Multispecies-UDRGM. An analysis of sensitivity to the table resolution has also been performed in order to evaluate the impact of subsequent refinement on the computational time and accuracy. This will be further discussed in next sections.
The properties (with corresponding units) needed to define the UDRGM for both liquid and vapor are:

- Density [kg m^{-3}]
- Enthalpy [J kg^{-1}]
- Entropy [J kg^{-1} K^{-1}]
- Specific heat at constant pressure [J kg^{-1} K^{-1}]
- Molecular weight (this is a constant value, so the lookup-table is not needed) [kg $kmol^{-1}$]
- Speed of sound [m s^{-1}]
- Viscosity [kg m^{-1} s^{-1}]
- Thermal conductivity [W m^{-1} K^{-1}]
- $\left(\frac{\partial \rho}{\partial T}\right)_{P=const.}$ [kg m^{-3} K^{-1}]
- $\left(\frac{\partial \rho}{\partial P}\right)_{T=const.}$ [kg m^{-3} Pa^{-1}]
- $\left(\frac{\partial h}{\partial T}\right)_{P=const.}$ [J kg^{-1} K^{-1}]
- $\left(\frac{\partial h}{\partial P}\right)_{T=const.}$ [J kg^{-1} Pa^{-1}]

3. NUMERICAL SETUP

The computational domain is a half of the 2D planar section of the nozzles tested by Nakagawa et al. [13]. Four geometries have been investigated in [13], which differ for the diverging angle of the nozzle. However, only the two geometries that have pressure trends above the triple point have been selected in the present study, namely nozzle A and B (although the Span and Wagner EOS can be extrapolated below the triple point, the possibility of ice formation demand for a deeper analysis and a specific study of the problem). A list of the tested inlet boundary condition is summarized in Table 1 for each nozzle. The representation of the Inlet boundary condition on the CO_2 P-h diagram is also visible in Figure 4.
The experimental data available from the work of Nakagawa et al. [13] are the static pressure and temperature at the side walls of the nozzle obtained from differential pressure gauge and thermocouple taps. The temperature trends were reported by Nakagawa et al. [13] as saturation pressures, assuming thermodynamic equilibrium. In the present study, these have been converted back into temperatures values in order to compare both pressure and temperature trends with the computational results.

Case	Θ [°]	Total Pressure [MPa]	Total Temperature [K]	α_v [-]
1	0.076	9.1	310.15	0.0
2		6.1	293.65	0.0
3	0.153	9.1	310.45	0.0
4		6.1	293.15	0.0

Table 1 Inlet boundary conditions

The main geometrical parameters as well as the diverging angles (θ) of the investigated nozzles are shown in Figure 5. Adiabatic Wall (with no slip condition) and Symmetry boundaries are adopted according to Figure 5. A two-equations k-ω SST turbulence model is selected for all the calculations.

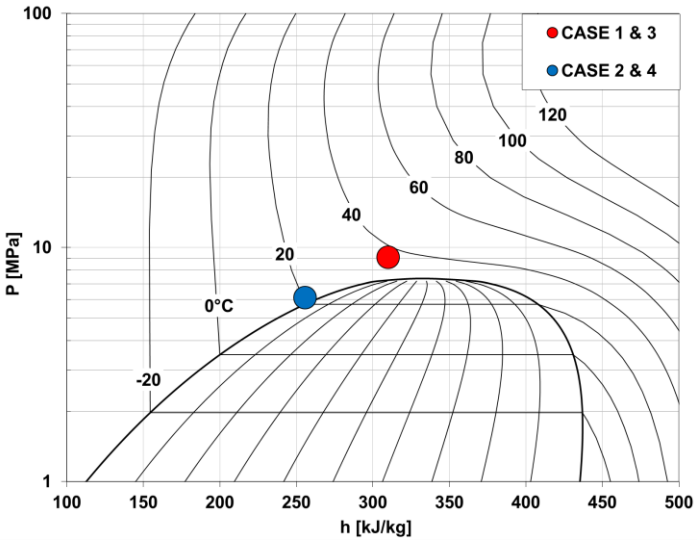

Figure 4 P-h diagram of CO_2 with representation of Nozzle Inlet boundary conditions

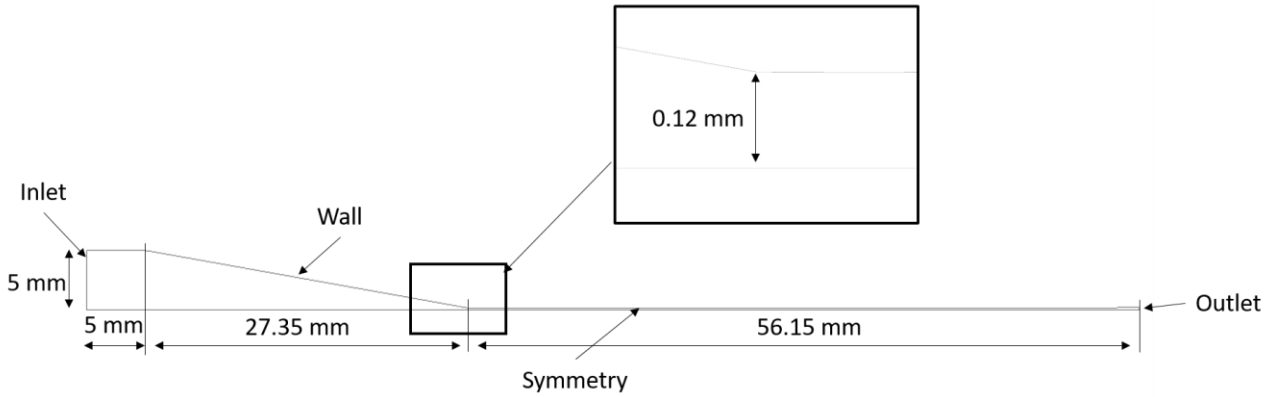

Figure 5 Nozzle Geometry with main quotes.
The outlet height are 0.195 mm and 10.27 mm corresponding to diverging angles (θ) of 0.076° and 0.153° respectively

The choice of 2D geometry was made in order to save computational cost. The 12000 quadrilateral elements mesh is shown in Figure 6. The values of wall y^+ are above 11 everywhere with the exception of the very beginning of the converging part of the nozzle where velocity is very slow. However, the k-ω SST in ANSYS fluent is based on a y^+ insensitive approach so that different values of this parameter along the domain do not affect the solution in a significant manner.
A pressure-inlet boundary condition has been used for the nozzle inlet. Several conditions have been tested at the outlet, as discussed in the next section. All the calculations have been performed using a pressure-based solver with pressure-velocity coupling. The discretization schemes are finally summarized in Table 2.

Discretization schemes adopted	
Quantity	**Method**
Gradients	Least Squares Cell Based
Pressure	PRESTO

All Others	3rd Order QUICK

Table 2 Numerical Setup Summary

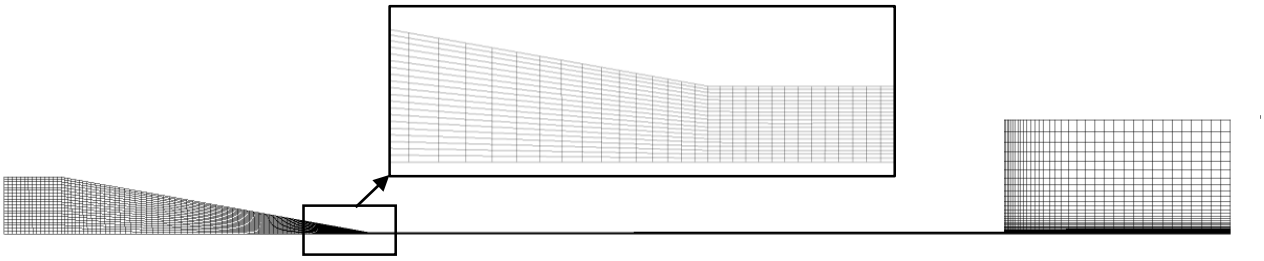

Figure 6 Computational Mesh with zoom near the nozzle throat

3.1 Sensitivity Analyses

Several preliminary calculations have been performed in order to test the model sensitivity to various numerical parameters:

- Mesh refinement;
- Lookup-tables refinement;
- Outlet geometry and boundary conditions;
- Evaporation factor σ_e

The condensation factor, σ_c, was found to have a negligible impact on the results, due to the scarce condensation occurring in the nozzle. Hence, a sensitivity analysis on this parameter has not been performed and will be addressed in future work related to full ejector CFD simulations, where the condensation factor is expected to have more influence.

The mesh sensitivity results are presented in Figure 7 for Case 2 of Table 1 (reference case) which shows a substantial equivalence of the three meshes with the exception of the plenum zone where the 50 000 elements mesh shows the presence of strong variations of pressure due to the mismatching of the nozzle exit pressure and imposed outlet pressure. Since the physics of the flow inside the plenum is not of interest in this work, the 12 000 elements mesh, also shown in Figure 6, was selected for all subsequent calculations.

The 12000 elements mesh analysis shows a good agreement with the experiments for both pressure and temperature and the values of the percentage errors for pressure and temperatures are shown in Table 3. As can be seen the agreement with measured temperatures is better than the one of pressures. In this latter case the CFD results are within the range of ±4.5% with the exception of the last pressure sensor; nevertheless, it is seen that for both pressure and temperature profiles, the experimental results are qualitatively well reproduced.

Percentage Errors		
P_1= 2.925 %	T_1 = -0.568 %	T_6 = -0.308 %
P_2 = 2.300 %	T_2 = -0.185 %	T_7 = -0.353 %
P_3 = -4.414 %	T_3 = -0.004 %	T_8 = -1.090 %
P_4 = -19.082 %	T_4 = -0.010 %	T_9 = -2.531 %
	T_5 = -0.243 %	

Table 3 Values of relative errors between CFD and Experiments. Sensors are numvered starting from the nozzle inlet.

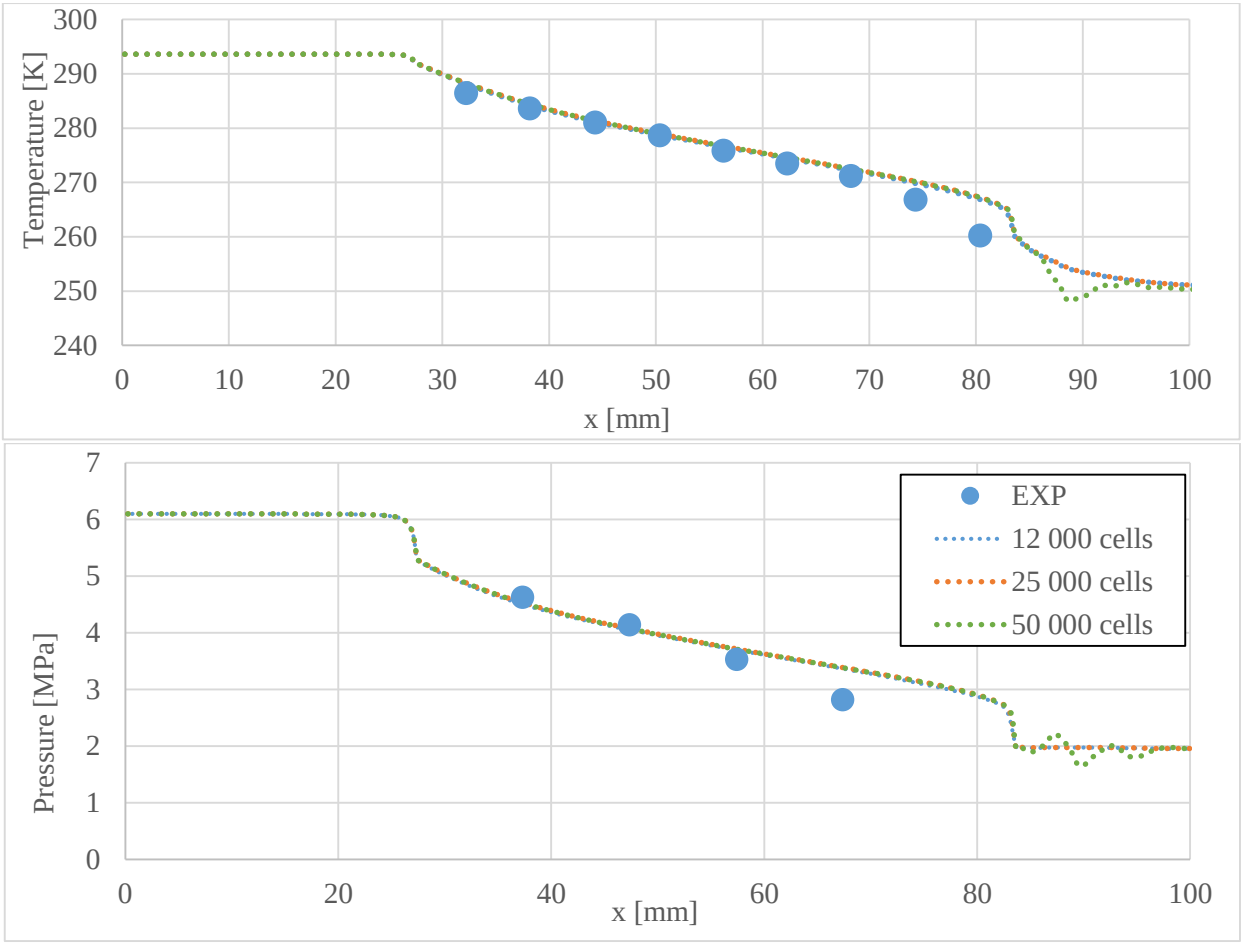

Figure 7 Mesh sensitivity. Symmetry data from the results of the geometry of Nozzle with Plenum

Figure 8 illustrates the effect of the refinement of the lookup tables for Case 2.
In the "Refined Tables" case, the lookup-tables were refined by approximately 5 times compared to the coarse case. Clearly, the results do not show significant variation between the two cases, with the 2 lines that are almost undistinguishable in the plots. By contrast, the computational time needed to achieve convergence increase by almost a factor of 4 for the refined case.
Table 4 shows the relative errors of the main thermodynamic quantities resulting from the CFD calculation with respect to the NIST Refprop libraries values for all the points along the nozzle symmetry axis. NIST values are calculated at the same pressure and temperature of the computed ones. The resulting errors, presented for both coarse and refined look-up tables, show a good agreement with respect to the values from Refprop database. The highest error that can be noted is for the vapor specific heat in case of coarse tables and is below 1.6% of absolute value.
Figure 9 shows the plot of liquid and vapor density along the nozzle axis of symmetry for the case of coarse look-up table. The corresponding NIST Refprop values, calculated at the same local pressure and temperature are also shown in the plot as well as the vapor volume fraction. The difference between computed and Refprop libraries values is negligible. Consequently, given also the advantage of reduced computational cost, the coarse tables have been preferred for all the calculations.

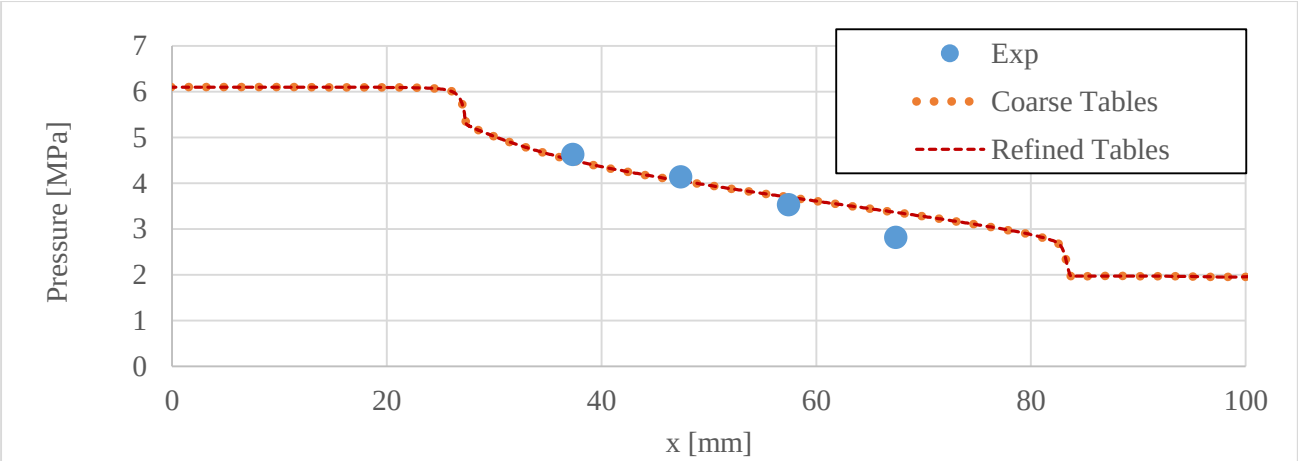

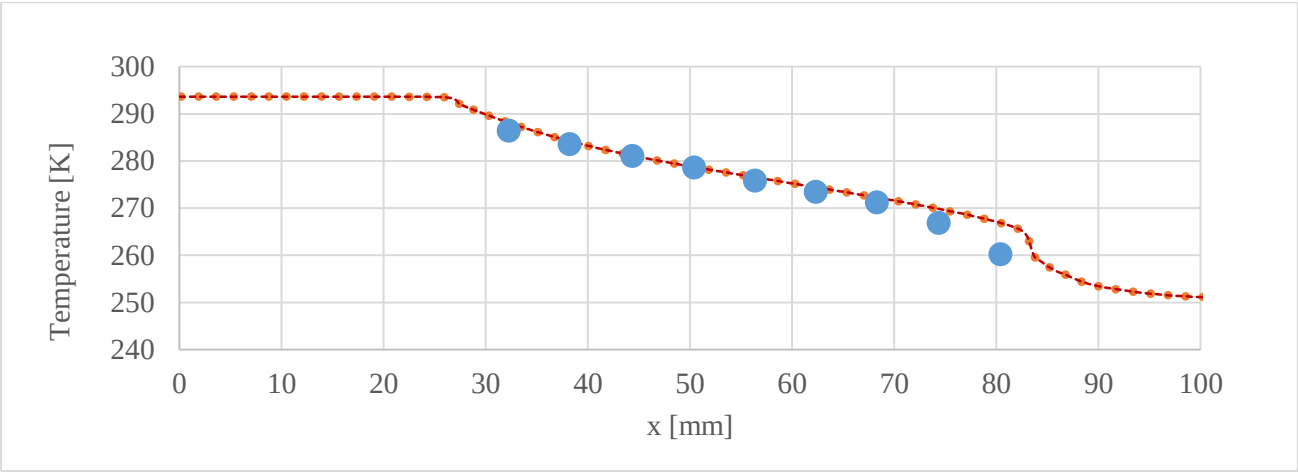

Figure 8 Tables refinement sensitivity. Symmetry data from the results of the geometry of Nozzle with Plenum

COARSE TABLES										
	LIQUID					VAPOR				
	ρ	***h***	***cp***	***k***	***μ***	***ρ***	***h***	***cp***	***k***	***μ***
MAX ERR [%]	0.04487	-0.00017	-0.00063	0.00623	0.05774	-0.00423	0.03298	-0.01704	-0.00535	-0.00074
MIN ERR [%]	0.00013	-0.02579	-0.71406	-0.01531	-0.00520	-0.15844	0.00057	-1.56289	-0.49593	-0.06385
AVERAGE ERR [%]	0.01097	-0.00691	-0.14024	0.00094	0.01194	-0.03804	0.00589	-0.19603	-0.06459	-0.00934
REFINED TABLES										
	LIQUID					VAPOR				
	ρ	***h***	***cp***	***k***	***μ***	***ρ***	***h***	***cp***	***k***	***μ***
MAX ERR [%]	0.00227	-0.00003	-0.00010	0.00024	0.00320	0.00222	0.00464	-0.00082	-0.00031	0.00031
MIN ERR [%]	0.00002	-0.00128	-0.03302	-0.00075	-0.00332	-0.02866	-0.00042	-0.17776	-0.05970	-0.00886
AVERAGE ERR [%]	0.00041	-0.00027	-0.00529	0.00003	0.00039	-0.00186	0.00027	-0.00937	-0.00314	-0.00047

Table 4 Maximum, Minimum and Average error of main thermodynamic quantities along the nozzle symmetry axis with respect to NIST Refprop libraries values.

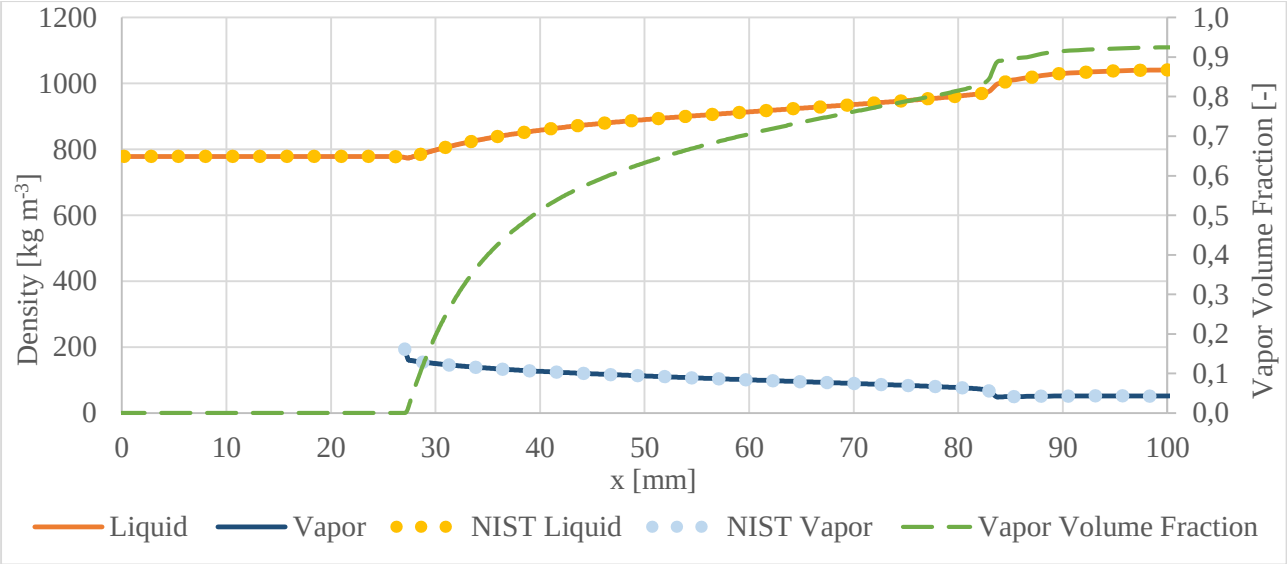

Figure 9 Density along the nozzle symmetry compared to NIST Refprop libraries results. The vapor volume fraction is also plotted.

Since the Mach number in a two-phase mixture does not have a univocal definition (a detailed discussion of this problem is given in section 4.3), the condition of supersonic chocked outflow was believed to be a potential issue. In order to check the presence of critical flow at the throat the mass-flow rate was verified to remain constant while varying the outlet pressure of the nozzle. In many cases, despite the Mach number at the outlet is supersonic, the absolute pressure of the flow was found to match the static pressure imposed at the boundary. This flow behavior is typical of subsonic regimes and is probably due to the inability of the software in properly evaluating the supersonic outlet conditions for a mixture flow.
Consequently, a sensitivity analysis was performed to investigate whereas different outlet boundary conditions (BC) and geometries could have an impact on the results. Three different conditions have been tested:

- Pressure-outlet BC imposed at the nozzle outlet without modification to the geometry of Figure 5;
- Addition of a plenum 20mm long and 10mm high with static pressure imposed at the plenum outlet;
- Addition of a diverging section with a diverging angle of 11.3° and static pressure imposed at the diverging section outlet.

Figure 10 illustrates the sketches of the different geometries tested.

Figure 10 Different tested outlet geometries

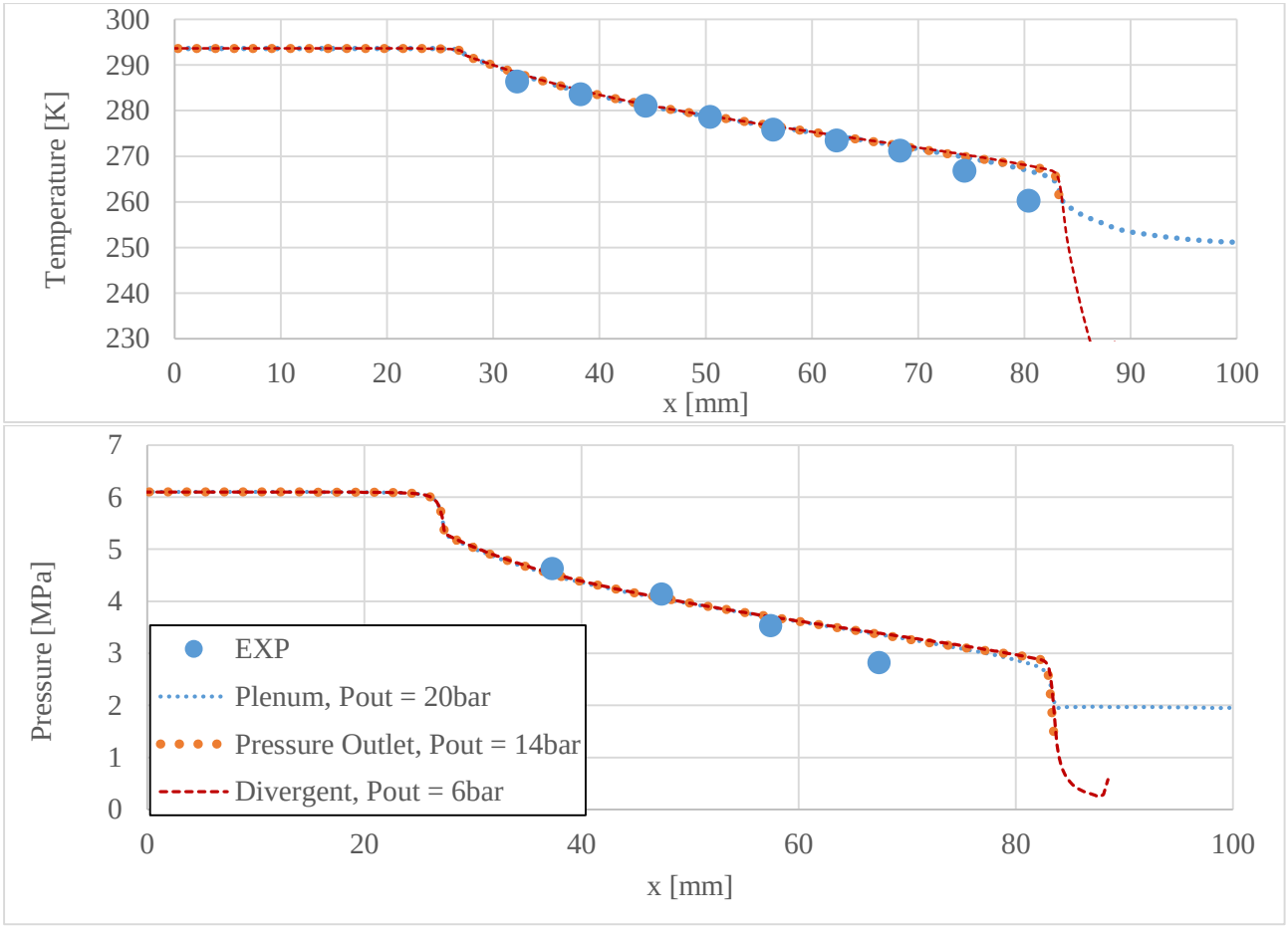

Figure 11 Outlet sensitivity analysis results. Symmetry data from the results of the different geometries of Nozzle with Plenum

The results of the comparison are presented in Figure 11. Both pressure and temperature profiles inside the nozzle (x < 85 mm) seem to be scarcely affected by the outlet geometry. The calculation of the plenum caused an increase in computational time and convergence instabilities due to the presence of unsteady flow features, such as recirculation at the plenum outlet and vortex shedding at the nozzle outlet. Nevertheless, the case with the plenum was considered to be the most reliable because no boundary condition has to be imposed at the nozzle outlet that affects the solution in unphysical ways. Moreover, a plenum is also present in the experimental set-up of Nakagawa et al. [13]. Consequently, all subsequent results refer to computational domains with a plenum at the outlet.

Finally, Figure 12 shows the effect of varying the evaporation factor for case 2. The comparison is made by varying by two order of magnitudes the value of the σ_e coefficient in Equation 7 (from $1x10^4$ up to $1x10^6$).

As can be seen, a lower value of the evaporation coefficient results in a higher temperature trend along the nozzle axis. This is particularly evident for $\sigma_e = 10000$ (blue line in Figure 12), although a slight difference can be also seen between the other two cases. This temperature variation depends on the latent heat that is absorbed by the flow when part of the CO_2 liquid mass evaporates.

In a similar way, the pressure decrease is generally more evident with a higher evaporation coefficient. This is due to the increase in vapor volume fraction, which leads to a significant acceleration of the mixture. In turn this causes a further pressure reduction due to the augmented friction losses.

For Case 2, the best agreement with experiments is achieved by imposing $\sigma_e = 10^5$ (orange dotted line in Figure 12). The same analysis was made for all the investigated cases and returned similar results. Therefore, only the solutions with $\sigma_e = 10^5$ will be presented in subsequent analyses.

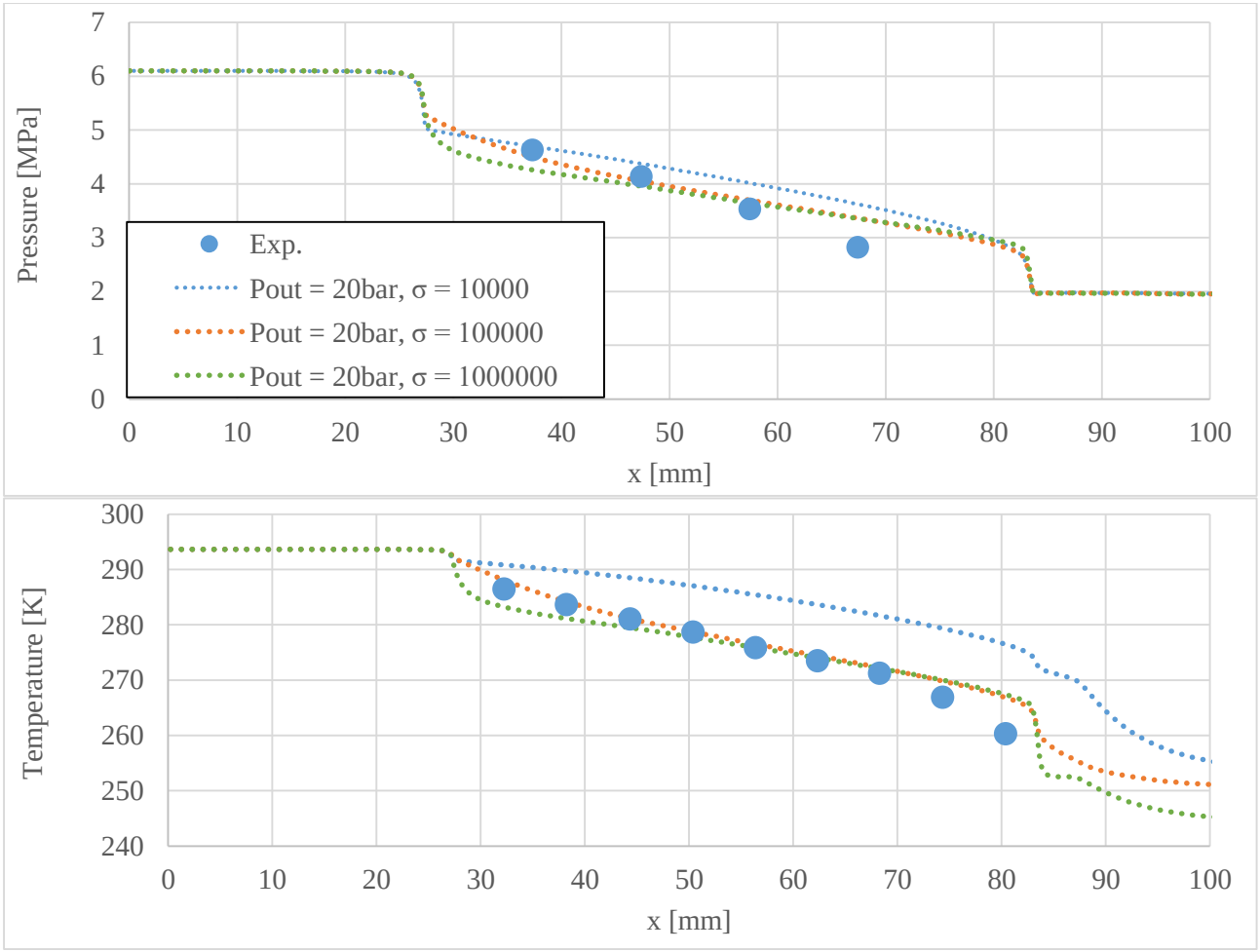

Figure 12 Evaporation coefficient sensitivity. Symmetry data from the results of the geometry of Nozzle with Plenum

4. RESULTS

4.1 Supercritical Inlet Condition

The comparison of numerical results and experiments for Case 1 are shown in Figure 13. The agreement with experimental data is good in the first half of the nozzle divergent, while the computed pressure and temperature are higher than the experiments in the second half of the nozzle length. These discrepancies are possibly due to an underestimation of the vapor volume fraction formed during the flashing process. Case 1 is the least accurate among all the presented cases. The maximum absolute values of relative errors for pressure and temperature, compared to the experimental values, are respectively: 34 % and 6.5%. In all the other cases lower percentage errors have been obtained.

Moreover, for this case it was found that the pressure and temperature go beyond the liquid phase spinodal limit in some cells. This problem is connected to the assumption of thermal and mechanical equilibrium between the phases. In particular, the Mixture-Model approach requires the use of a shared pressure and temperature between the phases. In cases where the CO_2 expansion is well within the saturation dome (e.g., qualities close to 0,5, such as in Case 1), the mixture state can cross regions where one of the two phases is beyond the Spinodal limit.

The adoption of a full Eulerian-Eulerian model should overcome this issue. Some preliminary tests, not presented in this paper, have been performed and will be the subject of subsequent studies.

Figure 14 shows the pressure and temperature trend for Case 3. Clearly, a better agreement with the experimental results is visible. However, a sudden pressure jump can be noted near the nozzle outlet, which is due to the presence of a shock-wave. This behavior is only visible in nozzle B, which has a larger diverging angle with respect to nozzle A. This issue will be further commented in the next section.

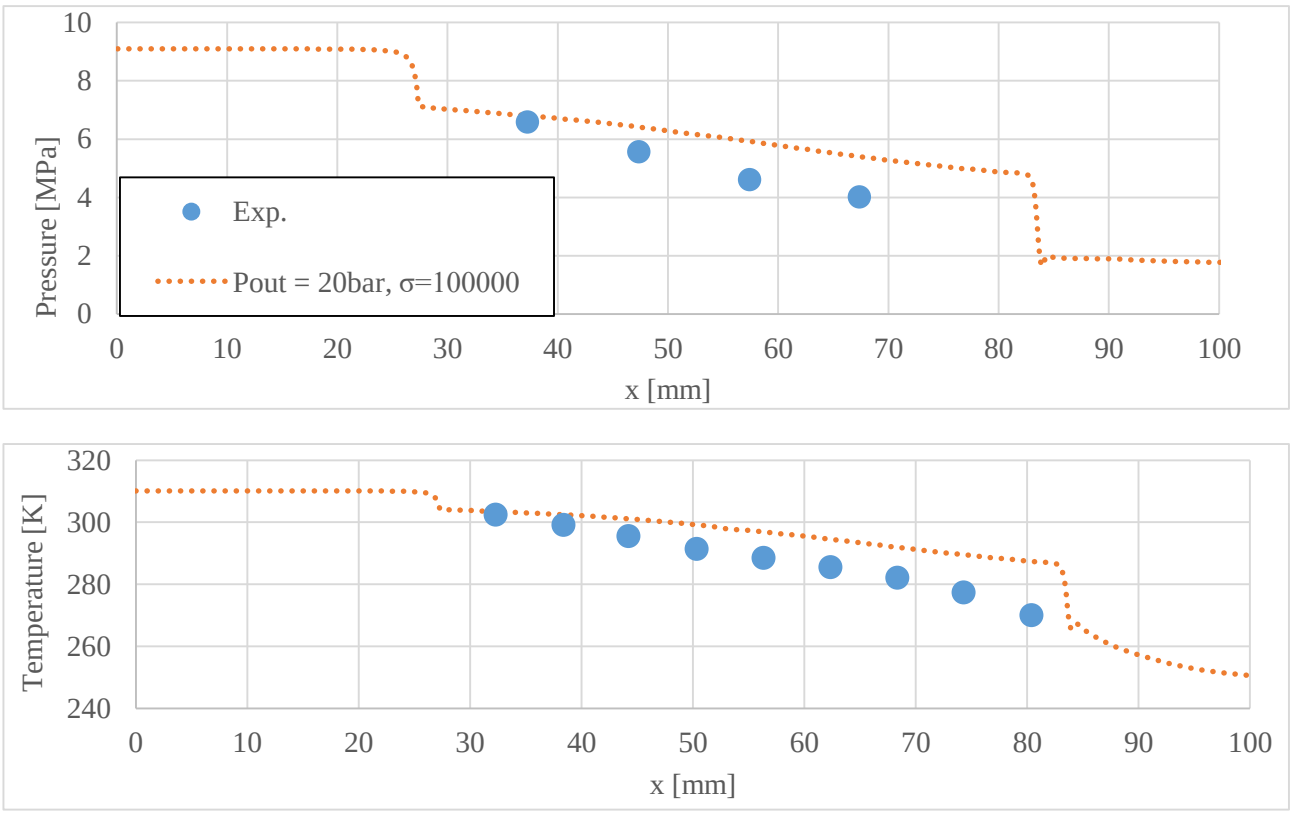

Figure 13 Case1. Numerical Results vs. Experiments (nozzle A)

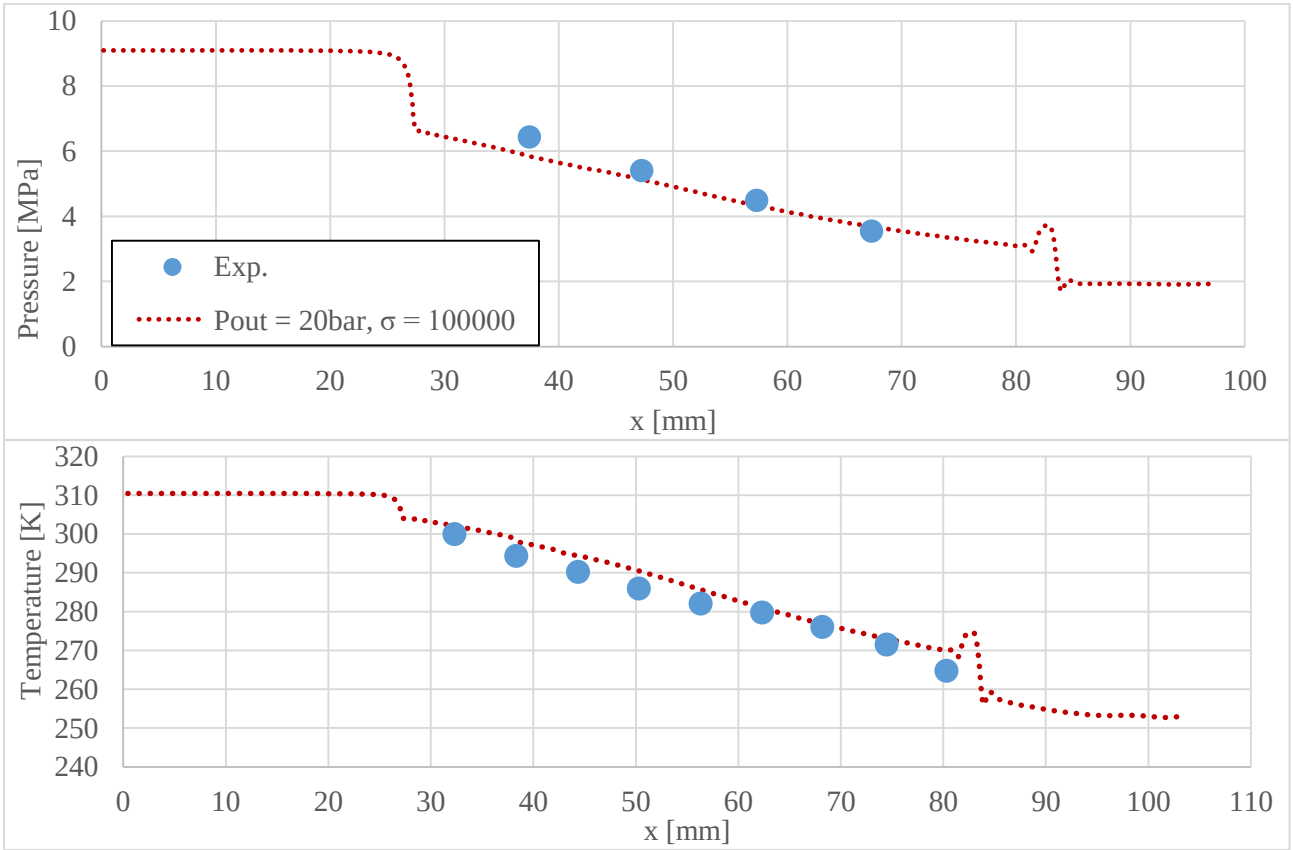

Figure 14 Case 3. Numerical Results vs. Expermients (nozzle B)

Figure 15 illustrates the contours comparison of vapor volume fraction, superheating and density gradient, between the two different tested geometries. In order to have a better visualization of the maps, the axial coordinate in all the contour plots has been scaled by $D_{th}/4$, where D_{th} is the throat hydraulic diameter. Moreover, only the divergent and the region close to the nozzle throat is showed.
The superheating is defined as the difference between the local temperature and the saturation temperature at the local pressure. When the superheating is above zero the liquid is in metastable state. Practically, this occurs all along the diverging part of the nozzle. In addition, it should be noted that in both cases the superheating reaches values above zero before the nozzle throat, although this is more evident in the contour of case 3.
The density gradient contour illustrates the regions of the computational domain where the phase change is more intense. In particular, the region with the highest density gradient is immediately downstream of the nozzle throat, where the wall corner induces a low pressure region that causes a significant flashing.
The direct comparison of two different geometries with similar inlet boundary conditions help visualizing the resulting differences caused by the wider diverging angle. For instance, the maximum value of vapor volume fraction is greater in case 3 because of the more abrupt expansion. Moreover, the nozzle outlet pressure is lower in case 3 and it causes the formation of a shock-wave near the nozzle exit. In turn, the shock-wave leads to a partial condensation of the vapor phase.

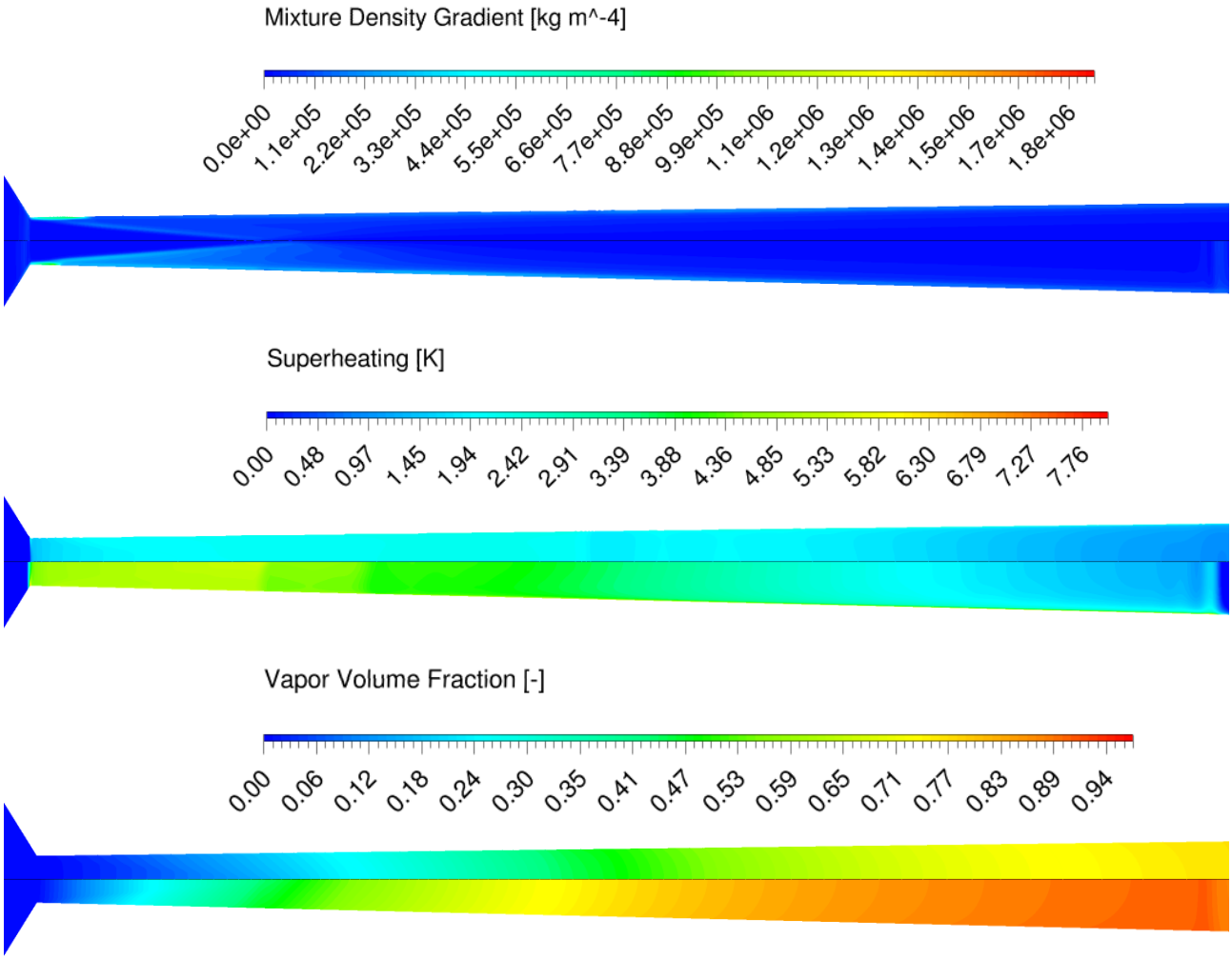

Figure 15 Case 1 (TOP) vs Case 3 (BOTTOM). Contour Comparison. (Out of scale)

4.2 Subcritical Inlet Condition

The numerical results of Case 2 have already been compared to the experiments in Section 2 and will not be repeated here. The results for Case 4 are presented in Figure 16. A good agreement with the experimental data is visible. As in Case 3 (which has the same geometry), a shock-wave appears near the nozzle exit.

According to the contours of Figure 17 the volume fraction after the shock-wave slightly decreases because of the condensation connected to the pressure rise. In this respect, a sensitivity analysis on the condensation factor σ_c may produce a better agreement of the results even with the last thermocouple of Figure 16.

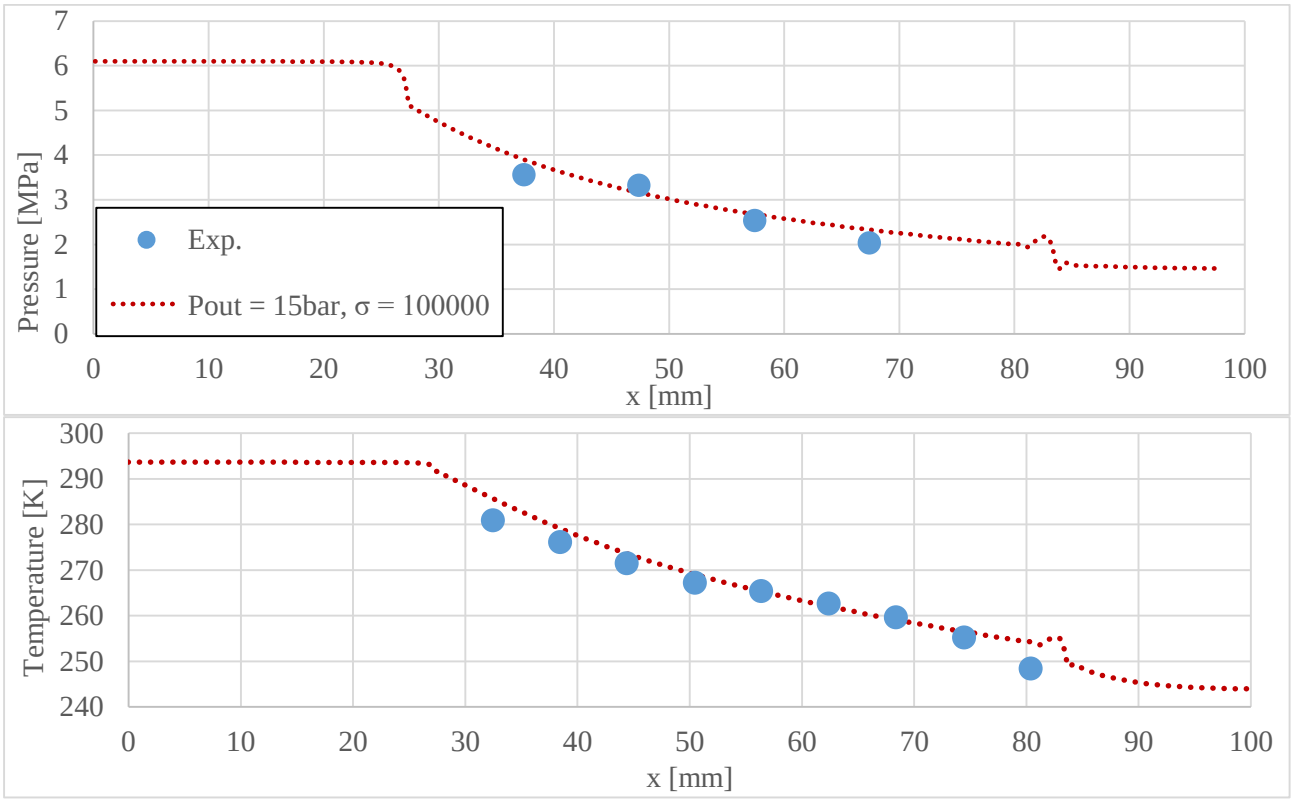

Figure 16 Case 4. Numerical Results vs. Experiments (nozzle B)

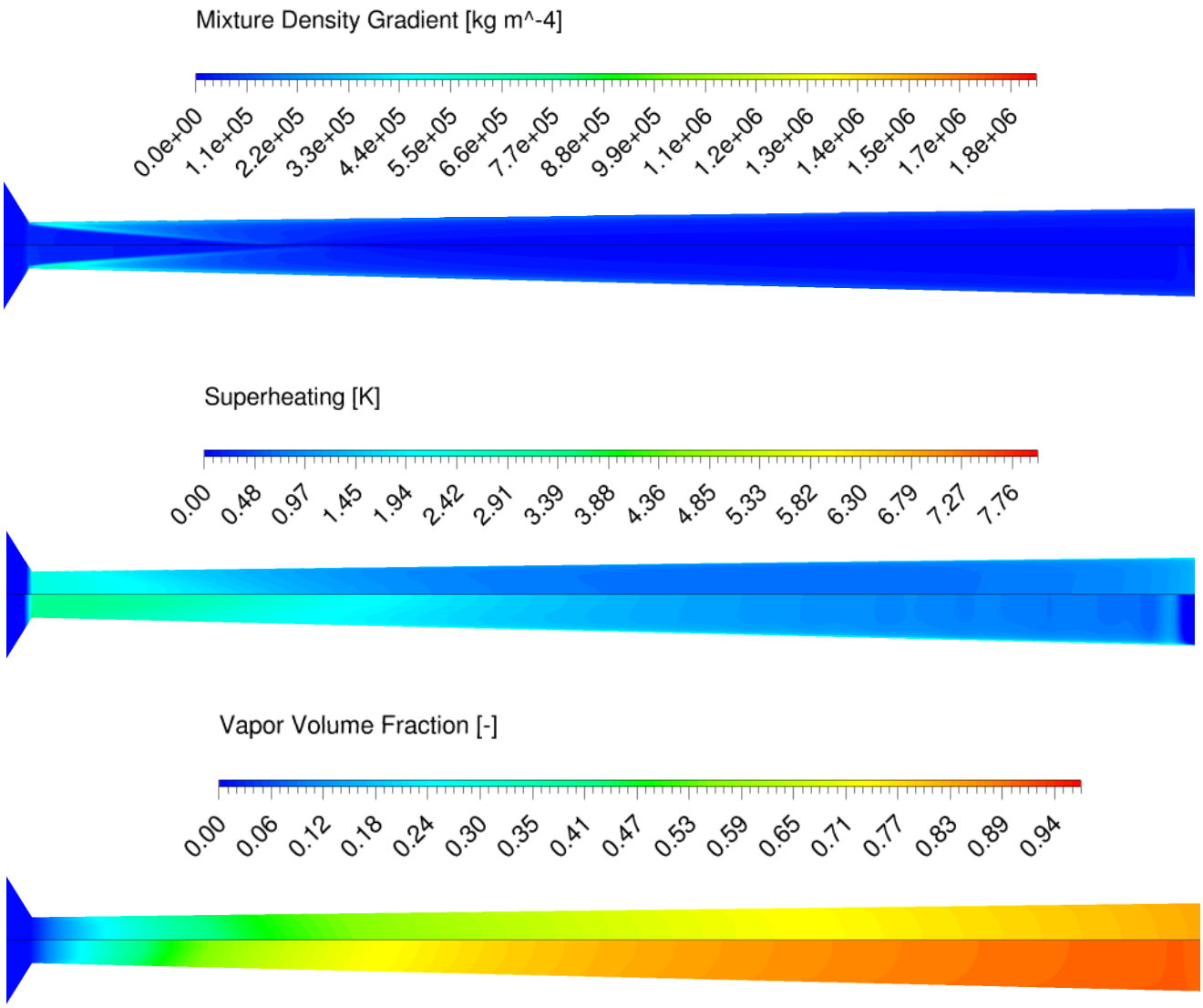

Figure 17 Case 2 (TOP) vs Case 4 (BOTTOM). Contour Comparison. (Out of scale)

4.3 Analysis of the mixture speed of sound

In order to analyze in greater detail the effect of the supersonic condition, the Mach number was calculated in post-processing by means of a different equation for the mixture speed of sound, in analogy to the work of Yazdani et al. [4].
The equation was derived by Brennen [29] by applying an incremental pressure to a mixture of liquid and vapor. It assumes homogeneous equilibrium model (instantaneous heat transfer between the phases) and homogeneous frozen model (no heat transfer between the phases) as extreme cases of validity.

$$\frac{1}{\rho a^2} = \frac{\alpha_v}{P}[(1-\varepsilon_v)f_v + \varepsilon_v g_v] + \frac{1-\alpha_v}{P}\varepsilon_l g_l \tag{8}$$

Where f and g are functions of the thermodynamic properties of the fluid while ε_v and ε_l are the interacting portions, i.e. portion of phase that exchange heat with each other, of vapor and liquid respectively. The equation was eventually simplified according to the suggestions of the same author:

- $f_v \approx 1$;
- $g_v \approx 1$;
- $\varepsilon_v \approx (1 - \alpha_v)$;
- $\varepsilon_l \approx \alpha_v$;
- $g_l \approx 2.1 \left(\frac{P}{P_{critical}}\right)^{-0.566}$

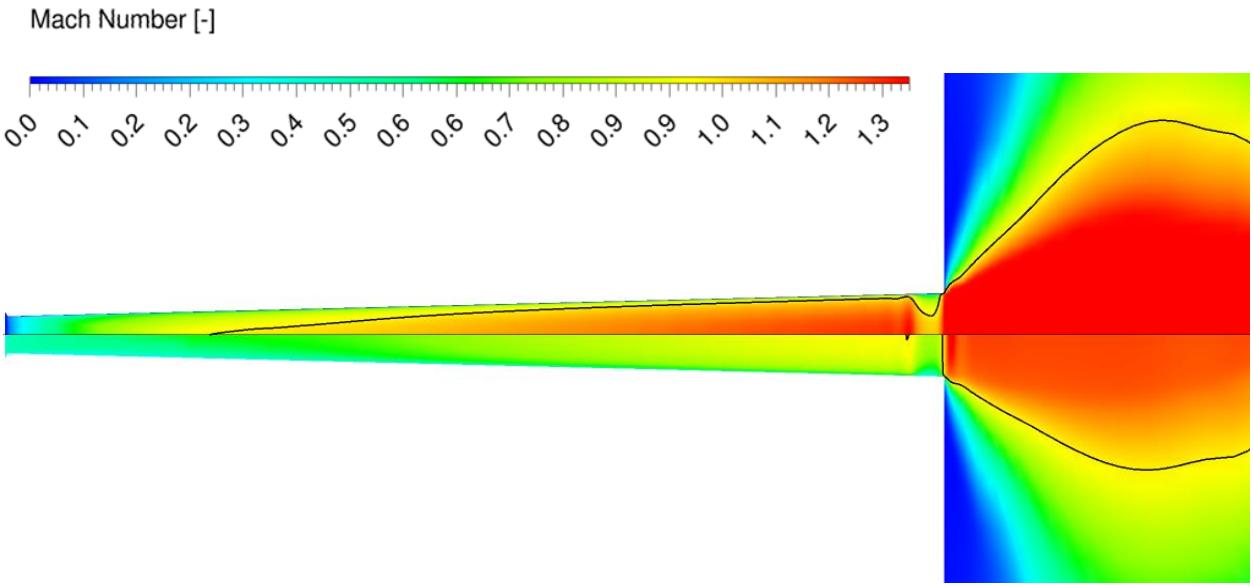

Figure 18 Case 3. Mach Number with Brennen Equation (TOP) vs Mach Number with Wallis Equation (BOTTOM) with sonic lines. (Out of scale)

In Figure 18 the contours of Mach Number calculated with the Brennen Equation (Equation 8) and the Wallis Equation (Equation 4) are compared along the nozzle diffuser and a portion of the plenum. The sonic lines of both cases are also visible.
The sonic line and Mach contour obtained with the Brennen equation seem to be in better agreement with the behavior of the flashing flow. In particular, the flow becomes supersonic in the diffuser and continues to accelerate until a shock-wave occurs, where a part of the flow becomes subsonic.
The contour obtained with Eq. 4 shows a similar trend with an abrupt acceleration that resemble a shock-wave. However, the Mach number in this case is below 1, which is in contrast with the predicted flow trend. Downstream of the nozzle exit plane, the jet spreading is clearly visible in both cases.
In this comparison the Wallis Equation for the mixture sound speed seems not completely appropriate to represent the mixture flow, resulting in Mach numbers that do not reflect the computational results. Perhaps, the issue in the proper evaluation of supersonic outlet condition (mentioned in section 3) could possibly be solved by implementing a different equation, similar to Equation 8, for the mixture speed of sound. Unfortunately, the Wallis expression is the default equation implemented in ANSYS Fluent and it cannot be modified by the user. According to ANSYS documentation [12] the speed of sound is used to solve the pressure-correction equation but further details are not available since it's not an open-source code.
Moreover, it should be noted that both the Wallis and Brennen equations are only "post-process" definition of the sound speed which in no way impact the final numerical solution. The actual numerical speed of sound stems mathematically from the governing systems of equations, and it depends on the choice of the equation of state [23].

5. CONCLUSIONS

The present paper describes a novel method to perform CFD calculations of flashing CO_2, implemented on the commercial solver ANSYS Fluent v.19.0 by means of *User-Defined-Functions*. The main feature of the method is the possibility of defining the properties of both phases by means of lookup-tables obtained from NIST Refprop v.9.1 libraries including liquid, vapor, supercritical and metastable states. This automatic procedure of implementing the properties is based on several VBA and C code functions and it can be easily adapted to virtually any kind of fluid in both single and two-phase flows.

The numerical simulations were compared to the experimental results available from literature with satisfactory agreement. The pressure and temperature profiles are qualitatively well reproduced except in Case 1, the least accurate among all the presented cases, where the maximum absolute values relative errors for pressure and temperature (with respect to the experimental values) are respectively: 34 % and 6.5%.

A comparison between two different equations for the mixture speed of sound has also been performed which illustrated that the Brennen formulation may be more accurate than the expression derived by Wallis and used as a default equation by commercial software adopted in this work.

REFERENCES

[1] G. Lorentzen, «Revival of carbon dioxide as a refrigerant,» *International Journal of Refrigeration,* pp. 292-301, 1993.

[2] S. Elbel e P. Hrnjak, «Experimental validation of a prototype ejector designed to reduce throttling losses encountered in transcritical R744 system operation,» *International Journal of Refrigeration,* pp. 411-422, 2008.

[3] S. Elbel e N. Lawrence, «Review of recent developments in advanced ejector technology,» *International Journal of Refrigeration,* pp. 1-18, 2016.

[4] M. Yazdani, A. A. Alahyari e T. Radcliff, «Numerical modeling of two-phase supersonic ejectors for work-recovery applications,» *International Journal of Heat and Mass Transfer,* pp. 5744-5753, 2012.

[5] C. Lucas, H. Rusche, A. Schroeder e J. Koehler, «Numerical investigation of a two-phase CO2 ejector,» *International Journal of Refrigeration,* pp. 154-166, 2014.

[6] J. Smolka, Z. Bulinski, A. Fic, A. J. Nowak, K. Banasiak e A. Hafner, «A computational model of a transcritical R744 ejector based on a homogeneous real fluid approach,» *Applied Mathematical Modelling,* pp. 1208-1224, 2013.

[7] F. Giacomelli, F. Mazzelli e A. Milazzo, «Evaporation in supersonic CO2 ejectors: analysis of theoretical and numerical models,» in *9th International Conference on Multiphase Flow*, Firenze, 2016.

[8] F. Giacomelli, K. Krzysztof Banasiak, A. Hafner, F. Mazzelli e A. Milazzo, «Experimental and Numerical Investigation on an Ejector for CO2 Vapor,» in *Gustav Lorentzen Conference* , 2018.

[9] The MathWorks Inc., MATLAB, version 8.6.0 (R2015b), Natick, Massachusetts, 2015.

[10] M. F. Colarossi, Multidimensional Modeling of Condensing Two-Phase Ejector Flow, University of Massachusetts Amherst, 2011.

[11] M. Haida, J. Smolka, A. Hafner, M. Palacz, K. Banasiak e A. J. Nowak, «Modified homogeneous relaxation model for the R744 trans-critical flow in a two-phase ejector,» *International Journal of Refrigeration,* vol. 85, pp. 314-333, 2018.

[12] ANSYS Inc., ANSYS Fluent Theory Guide, Canonsburg, PA: release 19.0, 2018.

[13] M. Nakagawa, M. S. Berana e A. Kishine, «Supersonic two-phase flow of CO2 through converging-diverging nozzles for the ejector refrigeration cycle,» *International Journal of Refrigeration,* vol. 32, pp. 1195-1202, 2009.

[14] F. Mazzelli, F. Giacomelli e A. Milazzo, «CFD modeling of condensing steam ejectors: Comparison with an experimental test-case,» *International Journal of Thermal Sciences,* vol. 127, pp. 7-18, 2018.

[15] C. E. Brennen, Cavitation and Bubble Dynamics, Oxford University Press, 1995.

[16] M. Labois e C. Narayanan, «Non-conservative pressure-based compressible formulation for multiphase flows with heat and mass transfer,» in *Proceedings of 9th International Conference on Multiphase Flow*, Firenze, 2016.

[17] G. Grazzini, A. Milazzo e F. Mazzelli, Ejectors for Efficient Refrigeration, Springer, 2018.

[18] V. P. Carey, Liquid-Vapor Phase-Change Phenomena, CRC Press, 2007.

[19] J. P. Janet, Y. Liao e D. Lucas, «Heterogeneous nucleation in CFD simulation of flashing flows in converging–diverging nozzles,» *International Journal of Multiphase Flow* , vol. 74 , p. 106–117, 2015.

[20] Q. Dang Le, R. Mereu, G. Besagni, V. Dossena e F. Inzoli, «Computational Fluid Dynamics Modelling of Flashing Flow in Convergent-Divergent Nozzle,» *Journal of Fluids Engineering,* 2017.

[21] Y. Liao e D. Lucas, «Possibilities and Limitations of CFD Simulation for Flashing Flow Scenarios in Nuclear Applications,» *Energies,* 2017.

[22] K. Karathanassis. I., P. Koukouvinis e M. Gavaises, «Comparative evaluation of phase-change mechanisms for the prediction of flashing flows,» *International Journal of Multiphase Flow,* n. 95, p. 257–270, 2017.

[23] M. De Lorenzo, P. Lafon, M. Di Matteo, M. Pelanti, J. M. Seynhaeve e Y. Bartosiewicz, «Homogeneous two-phase flow models and accurate steam-water table look-up method for fast transient simulations,» *International Journal of Multiphase Flow,* vol. 95, pp. 199-219, 2017.

[24] F. Giacomelli, G. Biferi, F. Mazzelli e A. Milazzo, «CFD modeling of the supersonic condensation inside a steam ejector,» *Energy Procedia,* pp. 1224-1231, 2016.

[25] Y. Fang, M. De Lorenzo, P. Lafon, S. Poncet e Y. Bartosiewicz, «An Accurate and Efficient Look-up Table Equation of State for Two-phase Compressible Flow Simulations of Carbon Dioxide,» *Industrial and Engineering Chemistry Research,* 2018.

[26] E. W. Lemmon, M. L. Huber e M. O. McLinden, *NIST Reference Fluid Thermodynamic and Transport Properties REFPROP - Users's Guide,* Gaithersburg, Maryland: U.S. Department of Commerce, 2013.

[27] R. Span e W. Wagner, «A New Equation of State for Carbon Dioxide Covering the Fluid Region from the Triple-Point Temperature to 1100K at Pressure up to 800MPa,» *J. Phys. Chem,* vol. 25, n. 6, pp. 1509-1595, 1996.

[28] F. Giacomelli, F. Mazzelli e A. Milazzo, «Evaporation in supersonic CO2 ejectors: analysis of theoretical and numerical models,» in *International Conference on Multiphase Flow*, Firenze, Italy, 2016.

[29] C. E. Brennen, Fundamentals of Multiphase Flows, Pasadena, California: Cambridge University Press, 2005.